Vol. 210: 1–12, 2001 | MARINE ECOLOGY PROGRESS SERIES
Mar Ecol Prog Ser | Published January 26

Boundary shear velocities and fluxes in the MEERC experimental ecosystems

Sean M. Crawford, Lawrence P. Sanford*

University of Maryland Center for Environmental Science, Horn Point Laboratory, PO Box 775, Cambridge, Maryland 21613, USA

ABSTRACT: Diffusion to solid-water interfaces is directly related to shear velocity. Shear velocities at the walls and bottoms of experimental ecosystem enclosures of different sizes and shapes (the Multiscale Experiment Ecosystem Research Center pelagic/benthic [MEERC P/B] tanks at the University of Maryland Center for Environmental Science, Horn Point Laboratory) were measured using hot-film sensors. Spatially averaged bottom and wall shear velocities were related to internal mixing, which was produced by rotating internal paddles and measured using a combination of gypsum dissolution and direct turbulence measurements. Shear velocities always increased with increasing mixing, but relationships between mixing and shear velocity changed with tank volume and shape. Spatially averaged bottom shear velocities decreased with increasing tank volume at an internal mixing level of 2 cm s^{-1}, but average wall shear velocities were similar for most tanks. In contrast, the rate of increase in bottom shear velocity with increasing mixing was similar for most tanks, but the rate of increase in wall shear velocity with increasing mixing was lower for the larger tanks. A bulk impeller Reynolds number captured some, but not all, of the scale dependence of ratios of boundary shear velocity to internal mixing intensity; mixing design and tank geometry were also important. Levels of all shear velocities in the MEERC P/B tanks were lower than levels in natural coastal environments for equivalent internal mixing. Realistic levels of internal mixing in the tanks resulted in unrealistically low boundary shear velocities. As a result, wall diffusive sublayer thicknesses were similar to those found in deep-sea environments, and benthic diffusive sublayer thicknesses were even larger. Most current mesocosm designs are likely to be affected similarly. The artificially low-energy benthic environment may have particularly important consequences for ecosystem processes affected by pelagic-benthic coupling.

KEY WORDS: Diffusion · Shear velocity · Interface · Experimental ecosystem · Mesocosm

INTRODUCTION

Most flows in nature are turbulent. In natural aquatic environments turbulence is created by wind shear at the surface, horizontal shear at the pycnocline and sediment surface, breaking surface and internal waves, and buoyancy effects such as convection. Turbulent mixing is important in natural aquatic ecosystems at scales ranging from planktonic interactions to mixing of large water masses with distinct physical properties. Another crucial aspect of natural turbulent mixing is its impact on fluxes of nutrients and wastes between different ecosystem compartments; e.g., across the sediment-water interface.

Turbulent mixing in experimental aquatic ecosystems also is important if they are to simulate natural ecosystem interactions adequately. In an experimental ecosystem enclosure the degree of mixing can greatly affect fluxes of nutrients, wastes, and dissolved gases not only throughout the water column but also to the benthic, air-water, and wall interfaces of the enclosure. Existing designs for mixing ecosystem enclosures allow some, but usually not all, aspects of natural mix-

*Corresponding author. E-mail: lsanford@hpl.umces.edu

ing to be mimicked (Sanford 1997). In stirred enclosures the water column may be realistically mixed but, in contrast to nature, enclosure turbulence is usually generated in the interior and not at the boundaries and there is little mean flow. This can lead to distorted boundary shears and flows, which can affect benthic organisms (Nowell & Jumars 1984, Snelgrove & Butman 1994) as well as mass transfer across interfaces, which is directly related to turbulent flow near the interface (Jørgensen & Revsbech 1985, Riber & Wetzel 1987, Hall et al. 1989, Jørgensen & Des Marais 1990, Santschi et al. 1991, Dade 1993). In flumes or benthic chambers, on the other hand, flow and shear at the benthic boundary may be realistic, while the flow in the water column is often too energetic (Porter 1999). These differences in turbulence characteristics between natural and experimental environments may be responsible for important differences in ecosystem function (Sanford 1997, Porter 1999).

Experimental ecosystem researchers need to know what artifacts are present in their enclosures. Understanding and accounting for these artifacts is essential for interpretation of results. This is one of the central themes of the Multiscale Experiment Ecosystem Research Center (MEERC) at the University of Maryland Center for Environmental Science. Measuring turbulence characteristics at the interfaces of experimental ecosystem enclosures and noting differences from the natural environment is thus an important aspect of experimental ecosystem research.

In this paper we report measurements of turbulent stresses at the wall and bottom boundaries of the MEERC experimental ecosystem enclosures. First a brief background is given on flow and diffusion across interfaces. This is followed by a description of the experimental enclosures used in this study and the results of previous internal mixing studies. This study's measurements of boundary shear velocities with hot-film sensors at different levels of interior mixing are then described. We conclude with a discussion of possible relationships between boundary shear velocities, experimental enclosure scale, and mixing design.

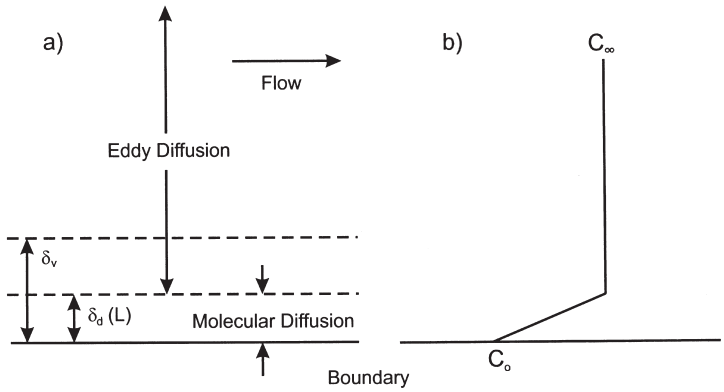

Fig. 1. Conceptual diagram of a diffusive sublayer in a smooth turbulent flow above a solid-water interface. (a) Diffusive sublayer δ_d (equivalent to film thickness L) is nested within the viscous sublayer δ_v; both δ_d and δ_v are inversely proportional to the shear velocity u_*; turbulent eddy diffusion controls mixing above δ_d and molecular diffusion dominates within the sublayer. (b) Result is a concentration profile reasonably approximated by a constant concentration C_∞ above the diffusive sublayer with a linear decrease to the interface concentration C_o within the sublayer

BACKGROUND

Flow and diffusion across interfaces

Turbulent energy enters aquatic systems at large scales. This energy is transferred down to smaller scales by the cascade of turbulent energy (Batchelor 1967). A simple way to describe turbulent mixing of momentum at large scales is to use a larger viscosity representing the influence of the large turbulent eddies, known as the eddy viscosity. Similarly, mass transfer takes place by eddy diffusion in turbulent flows (Sanford 1997).

Near interfaces and at smaller scales, molecular diffusion becomes the dominant form of mass transfer (Jørgensen & Revsbech 1985). Applying Fick's first law of diffusion, geochemists relate the flux of any scalar (e.g., dissolved gases, nutrients, temperature) to/from a boundary to the concentration difference across a film of thickness, L, dominated by molecular diffusion:

$$F = \frac{D\Delta C}{L} \quad (1)$$

where F is the scalar flux in g cm^{-2} s^{-1}, ΔC is the change in scalar concentration in g cm^{-3}, D is molecular diffusivity in cm^2 s^{-1}, and L is measured in cm (Fig. 1). This film thickness often is considered to be equivalent to the diffusive sublayer thickness, δ_d, which is directly related to the turbulent flow above the boundary (Jørgensen & Revsbech 1985, Riber & Wetzel 1987, Hall et al. 1989, Jørgensen & Des Marais 1990, Santschi et al. 1991, Dade 1993).

The diffusive sublayer is nested at the bottom of the viscous sublayer, δ_v, which is itself the lowest region of a smooth turbulent boundary layer flow (Fig. 1). The viscous sublayer is the region where viscosity damps out turbulence and dominates momentum transfer. It is related to the properties of the turbulent flow and the fluid by

$$\delta_\nu = 10\frac{\nu}{u_*} \quad (2)$$

where $u_* = (\tau_b/\rho)^{1/2}$ is the boundary shear velocity, τ_b is the boundary shear stress in g cm^{-1} s^{-2}, ρ is the density of water in g cm^{-3}, $\nu = \mu/\rho$ is the kinematic viscosity in cm^2 s^{-1}, and μ is the dynamic viscosity in g cm^{-1} s^{-1}. A viscous sublayer is present as long as the interface roughness is small compared to the viscous sublayer thickness (Rahm & Svensson 1989) This is often the case over muddy bottoms, in low-energy environments, and at the walls and benthos of experimental ecosystems.

Molecular diffusivity in water is not as effective at smoothing out scalar gradients as is viscosity at smoothing out velocity gradients. Therefore, the diffusive sublayer is usually smaller than the viscous sublayer and its thickness is given by

$$\delta_d = Sc^{-\frac{1}{3}}\,\delta_\nu \quad (3)$$

where Sc is the Schmidt number, $Sc = \nu/D$. As the Schmidt number becomes larger (by D decreasing) the diffusive sublayer becomes smaller relative to the viscous sublayer (Jørgensen & Revsbech 1985). Combining Eqs. (2) & (3) yields an expression for δ_d in terms of the molecular properties of the fluid and u_*:

$$\delta_d = \frac{10D\,Sc^{\frac{2}{3}}}{u_*} \quad (4)$$

from which it is apparent that increasing u_* decreases δ_d and decreases fluid resistance to boundary fluxes (substituting Eq. [4] into Eq. [1]). Thus, the shear velocity u_* is the most important turbulence parameter for boundary fluxes.

Previous mixing measurements in MEERC

The work presented here was conducted as part of the MEERC program, which was committed to investigating scaling effects in experimental ecosystem enclosures. This work was done in the MEERC pelagic/benthic (P/B) tanks which are made up of 5 series of tanks of different scale (designated as A, B, C, D, and E in order of increasing diameter). MEERC P/B tank dimensions and relative shapes are given in Table 1 and Fig. 2. Mixing is achieved by large slow-moving paddles which mix the water column completely and at realistic levels of interior turbulence. To prevent the development of plug flow, these paddles rotate 7.5 times in one direction, stop for 15 s, and rotate 7.5 times in the other direction. Interior mixing characteristics and measurement techniques have been described briefly in Petersen et al. (1998) and Porter (1999), and are summarized below. Levels of shear at the wall and bottom boundaries had not been measured or reported prior to this work, but were thought to be lower than in natural ecosystems. Quantification of these boundary shears and their relationships to interior mixing were the goals of the present research.

Two techniques were used to quantify interior mixing in the MEERC P/B tanks. Gypsum dissolution experiments were conducted prior to the first ecosystem experiments. The gypsum dissolution experiments used 2 different mixing rates in each series, except in the D tank, where 3 mixing rates were used (Table 1). Gypsum balls were placed throughout the tanks (Fig. 3), and the weight loss from each was measured after mixing at the rotation rates given in Table 1. The results of these dissolution studies were used to set the mixing rates for the MEERC P/B experiments in an attempt to match turbulence levels across all tanks. Gypsum dissolution was used because no other techniques for measuring turbulence characteristics were available at the time.

Subsequently, direct measurements of turbulent velocities were made in the D tanks using a Sontek acoustic doppler velocimeter (ADV; Kraus et al. 1994). The locations of these ADV measurements corresponded to the locations of 5 selected gypsum balls from the previous dissolution experiment (Fig. 3), and they were carried out at the same mixing rates as the dissolution experiments. These turbulence measurements were used to calibrate the gypsum dissolution technique. Two measures of mixing intensity were calculated. The first was the total root mean-square velocity, which included the mean flow in the calculation

$$U_{rms,tot} = \sqrt{\frac{1}{3}\left(u_{rms}^2 + v_{rms}^2 + w_{rms}^2\right)} \quad (5)$$

where u_{rms}, v_{rms}, and w_{rms} are the total root mean-square velocities in the x, y, and z directions. The second measure was the root mean-square velocity with

Table 1. MEERC P/B tank dimensions and experimental mixing rates (rpm)

Tank series	Diam. (m)	Height (m)	Vol. (m^3)	rpm
A	0.35	1.00	0.1	7.5, 22.5
B	0.52	0.46	0.1	7.5, 22.5
C	1.13	1.00	1.0	3.75, 7.5
D	2.44	2.15	10.0	2, 3.75, 6
E	3.57	1.00	10.0	2, 6

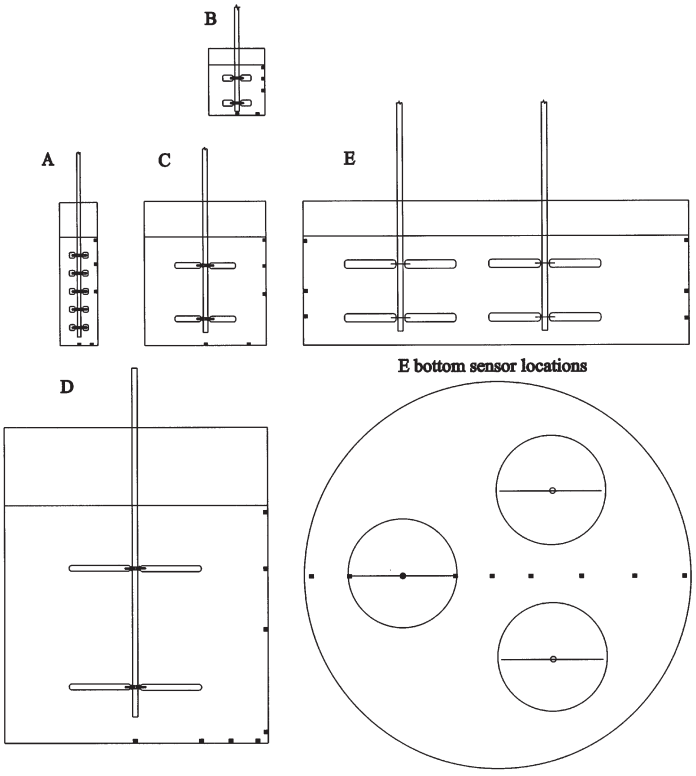

Fig. 2. Scale diagram of the MEERC P/B tanks and hot-film sensor locations. Only profile views of the cylindrical tanks are shown here, except for the E tank. Tank dimensions and volumes are given in Table 1

the mean removed, defined by Tennekes & Lumley (1972) as the most appropriate scale for turbulent intensity. Because the fluctuating components of velocity were usually greater than the mean components of velocity in the MEERC tanks, the 2 measures of mixing intensity are almost the same. We use $U_{rms,tot}$ here because both the mean flow and the fluctuating flow contribute to shear at the boundaries of the tanks. The regression which allows conversion of gypsum dissolution rate to $U_{rms,tot}$ for all the MEERC tanks is presented in Fig. 3b and is given by

$$d = 0.074 + 0.053 U_{rms,tot} \quad (6)$$

($r^2 = 0.95$), where d is dissolution rate in g h^{-1} and $U_{rms,tot}$ is in cm s^{-1}. This regression was used to estimate mixing intensity in all the MEERC P/B tanks, converting measured gypsum dissolution rates in each tank to estimates of $U_{rms,tot}$ using Eq. (6). The use of gypsum dissolution to estimate mixing intensity was considered acceptable in this case because ratios of fluctuating flow to mean flow were similar in all of the tanks (Porter et al. 2000). The $U_{rms,tot}$ estimates were interpolated throughout each tank using the Kriging technique in Surfer (Golden Software, Golden, CO, USA). Example contour

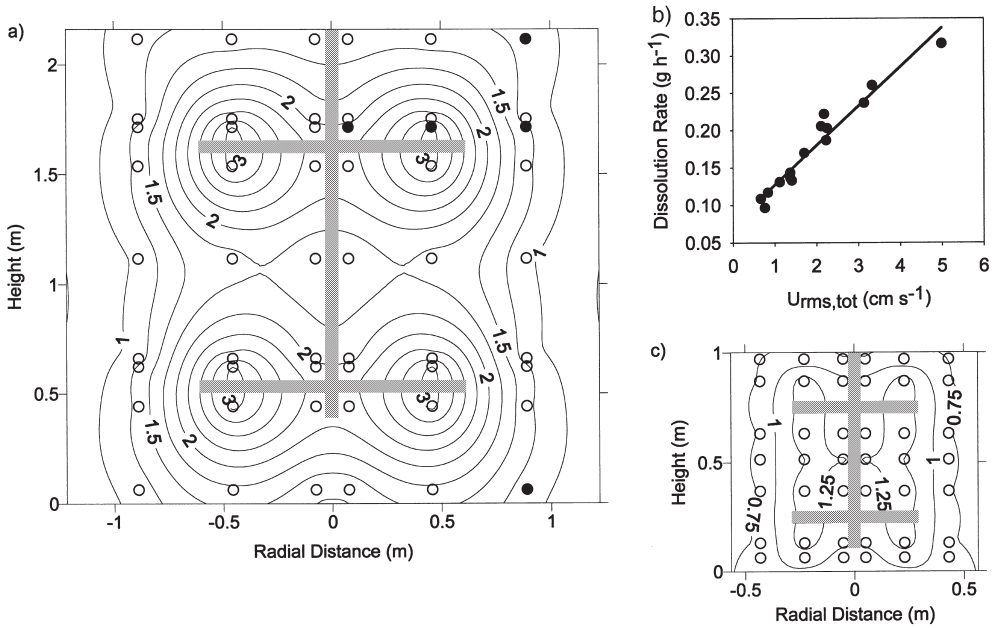

Fig. 3. Contours of $U_{rms,tot}$ (mixing intensity) at 3.75 rpm in the D tank (a) and C tank (c). (○) Data points from gypsum-dissolution experiments. ● in panel a: locations with both acoustic Doppler velocimeter measurements and gypsum-dissolution measurements, from which the gypsum dissolution calibration curve in (b) was derived. Contours of $U_{rms,tot}$ in cm s^{-1} were derived by applying this calibration to the gypsum dissolution data. Paddles are indicated in grey

Table 2. Weighted average internal $U_{rms,tot}$ (mixing intensity) velocities, weighted average shear velocities ($\bar{u}_*$) and standard deviations for wall and bottom boundaries. All velocity units are in cm s^{-1}

Tank	rpm	$U_{rms,tot}$	Wall		Bottom	
			$\bar{u}_*$	σ	$\bar{u}_*$	σ
A	7.5	0.690	0.082	0.005	0.129	0.016
	22.5	2.410	0.177	0.021	0.224	0.035
B	7.5	1.353	0.225	0.081	0.094	0.054
	22.5	5.267	0.777	0.142	0.694	0.053
C	3.75	0.944	0.109	0.019	0.134	0.038
	7.5	1.736	0.127	0.019	0.149	0.042
D	2	0.770	0.086	0.004	0.036	0.003
	3.75	1.507	0.098	0.008	0.053	0.005
	6	3.082	0.108	0.011	0.107	0.013
E	2	0.981	0.139	0.020	0.062	0.016
	6	4.214	0.203	0.031	0.200	0.032

plots of interpolated $U_{rms,tot}$ at 3.75 rpm in the C and D tanks are presented in Fig. 3. Weighted average $U_{rms,tot}$ values were subsequently calculated for all tank and mixing rate combinations using cylindrical volume weighting. The final calculated average values are presented in Table 2.

METHODS

For the present research, a series of experiments were devised to measure shear velocities in the MEERC P/B tanks in relationship to interior mixing. Measuring the friction velocity, u_*, can be done economically with hot-film sensors (Gust 1988), or by the dissolution of gypsum plates (Santschi et al. 1991). There are advantages and disadvantages to using either method. Hot-film sensors can measure the friction velocity at a high frequency response and small spatial resolution, but they require precise calibration. They also require a minimum threshold shear velocity for consistent performance (Gust 1988). The gypsum dissolution method is simpler, but is extremely labor intensive and gives only an average measure of friction velocity. We chose to use hot-film sensors for our experiments.

The sensors were manufactured by Micro Measurements (Raleigh, NC, USA) Type WTG-50A, and were connected to individual TSI, Inc. anemometer cards which were, in turn, connected to a datalogger. A Tattletale datalogger, Model 2B, was used to record measurements at 20 Hz. Hot-film sensors measure shear velocity by constant temperature hot-film anemometry as described by Gust (1988) at a 1.05 overheat ratio. Calibration of the sensors was done using a 40 cm microcosm (Gust & Muller 1997) which, when set at a specific rotating speed and pumping rate, produces a nearly homogenous shear velocity across its bottom. The lowest calibrated shear velocity setting of the microcosm was 0.288 cm s^{-1}. This corresponded to different voltages for each sensor, depending on the sensor's resistance and its sensitivity to changes in shear velocity.

In many cases the raw voltages measured in the MEERC P/B tanks fell below this threshold value on the original calibration curves. This occurred mostly at low mixing rates in the larger tanks. Much effort was made to extend the calibration curves to these lower values. The following technique was ultimately chosen: the lowest repeated instantaneous voltage measured for each sensor during the actual experiments was chosen to represent zero shear velocity. This was believed to be a reasonable approximation because repeated instantaneously low readings were thought to be more representative of instantaneous zero shear velocity, unaffected by convection from the sensors that develops in still water. When calibration curves included these points they fit a linear theoretical relationship between $u_*^{2/3}$ and voltage E^2 (Gust 1988) quite well, with r^2 values ranging from 0.97 to 0.99. Example calibration curves are shown in Fig. 4. The raw voltage data were transformed into shear velocities using these calibration curves.

Sensors were mounted flush to the walls and bottoms of the tanks so they disrupted the smooth boundary flow as little as possible. This was done to ensure that the boundary layer of the interface was measured and not that of the sensor. The sensors were developed for use in gases rather than liquids. Therefore, the sensor leads had to be covered by approximately 1 mm of thin flexible plastic for underwater use in the tanks. Silicon cement was used to attach the sensors to the walls and bottoms of the tanks, and to smooth the transition between tank and sensor. Sensors generally protruded less than a total of 2 mm from the surrounding surface, significantly less than the typical thickness of the viscous sublayer on the walls and bottom of the tanks (~1 cm).

The tanks selected from each series for the hot-film sensor experiments were the same ones used for the previous gypsum dissolution rate experiments and direct turbulence measurements. Tanks A1, B1, C1, D2, and E1 were used. The same mixing regimes used in previous experiments were used here so results could be compared. The rotation rates used are given in Table 1.

The locations of measuring points depended on tank geometry and paddle position. Fig. 2 shows the sensor locations in the tanks from each series. In the A, B, and C tanks, 3 locations were measured on the walls: at the

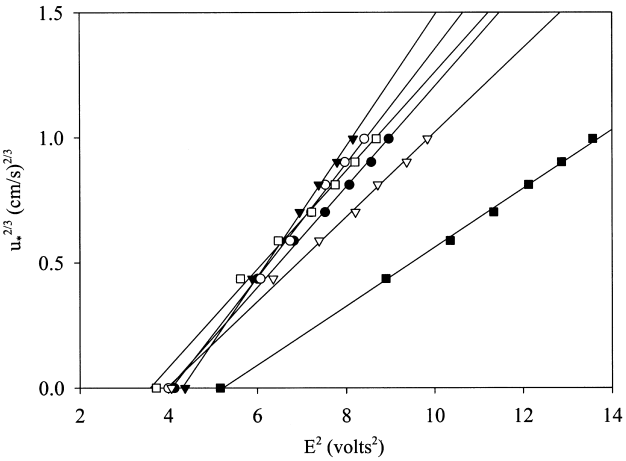

Fig. 4. Examples of calibration curves for hot-film sensors at different temperatures, including extrapolation to zero shear velocity. r^2 values ranged from 0.97 to 0.99 for all sensors at all temperatures

water surface, between paddles, and adjacent to a paddle. Two locations were also measured on the bottom of the tanks, at the center and two-thirds of the radius from the center. In the D tanks, 4 locations were measured on the walls: the surface, adjacent to a paddle, between paddles, and 10 cm off the bottom. On the bottom of the D tank, 4 measurements were made: at the middle, one-half radius, three-quarter radius, and 10 cm off the wall. Sensors were not placed in the corner where the bottom meets the wall because this is a small area in the tank where flow is uncharacteristic and it may incorrectly weight the spatial average. In the E tanks, which had 3 sets of mixers, 2 sets of 3 sites were measured on the walls, spaced vertically as in the A, B, and C tanks; 1 vertical set was adjacent to a mixer and 1 was between 2 mixers. On the bottom of the E tank, 2 radial lines were measured with spacing similar to the D tanks, but 1 line was under a mixer, and 1 was between 2 mixers. Measurements were replicated by moving the sensors around the tanks to similar locations relative to the mixing paddles and repeating the experiment.

Spatially weighted average shear velocities for the wall and bottom boundaries were calculated using weights based on the area of wall or bottom represented by each set of measurements. Because shear velocity data were distributed log-normally (see 'Results'), weighted average geometric means and standard deviations (Langley 1968) were calculated. Relationships between boundary u_*'s and water column $U_{rms,tot}$'s were examined for scale-dependent patterns. Analyses of covariance were performed using SAS 6.0 (SAS Institute, Inc., Carey, NC, USA) to determine if there were significant differences between the tanks in mean levels of shear velocity adjusted (by linear interpolation or extrapolation) to a common internal mixing-intensity level of $U_{rms,tot}$ = 2.1 cm s^{-1}. Tests for significant differences between tanks in the slopes of the u_* versus $U_{rms,tot}$ regression lines were also conducted. The statistics are reported at a 95% confidence interval unless otherwise noted. Of the 5 tanks, 4 had data collected at only 2 levels of $U_{rms,tot}$, such that a linear fit between the 2 values was the only possible choice. However, the D tanks had data collected at 3 mixing rates, which allowed the assumption of linearity to be tested.

RESULTS

An example time series of raw hot-film sensor voltage data is shown in Fig. 5. This data was collected at the bottom boundary of the C tank at two-thirds radius (0.33 m) from the center at 7.5 rpm, a high experimental mixing rate. The time series of voltage were converted to shear velocity using previously derived calibrations. The frequency distribution of u_* corresponding to the voltage time series of Fig. 5, was approximately log-normal (Fig. 6), which was true for almost all of the data collected. The 150 s cycles in the time series data in Fig. 5 are due to the 150 s cycle of paddle rotation (7.5 revolutions updraft at 7.5 rpm, 15 s pause, 7.5 revolutions downdraft at 7.5 rpm, 15 s pause). The reversing circulation in the tank clearly

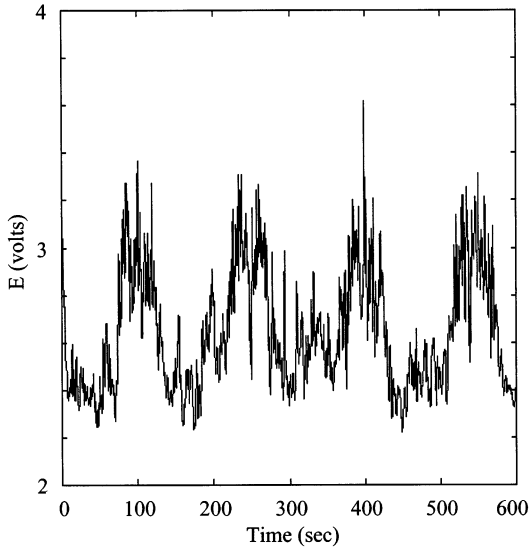

Fig. 5. Example of a time series of raw voltage data from Hot-Film Sensor 1 at the bottom boundary of the C tank at two-thirds radius from the center at 7.5 rpm, a high experimental mixing rate. Cycles in the data correspond to changes in the paddle direction of rotation, which create alternating upwelling and downwelling circulations and corresponding large changes in u_*

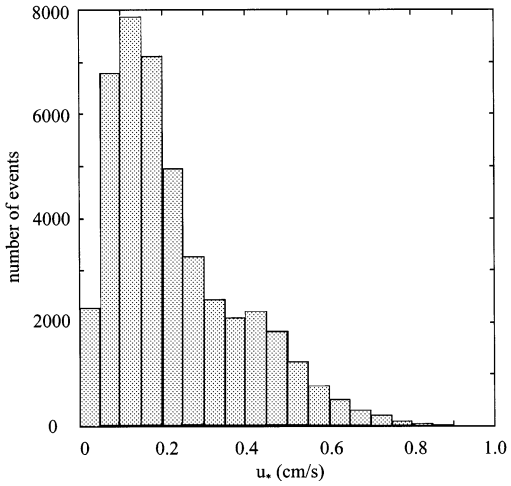

Fig. 6. Example histogram of shear velocity (u_*) at the bottom boundary of C tank at two-thirds radius from the center at 7.5 rpm. Shear velocity data followed a log-normal distribution

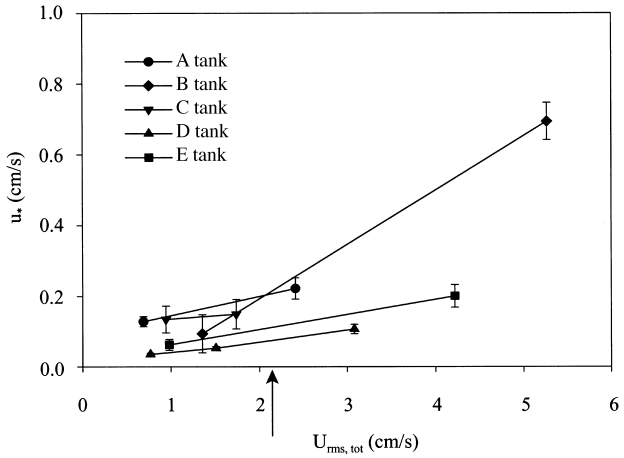

Fig. 7. Shear velocity (u_*) measured by hot-film sensors at the bottom boundary versus mixing intensity ($U_{rms,tot}$) in the MEERC P/B tanks. Weighted average geometric means and standard deviations from 4 experimental runs per tank are shown; arrow shows the normalizing level for comparison of mean shear velocity between tanks

resulted in an asymmetrical response at the bottom boundary; u_* values ranged from lows near 0 (at E ≈ 2.25 V) to highs >0.8 cm s^{-1} , with a geometric mean (median) value of approximately 0.15 cm s^{-1}. Data from this high mixing rate are presented here to show an example with highly variable u_*. At the lower mixing rates used in operational MEERC ecosystem experiments, temporal variability of u_* was not as marked.

However, this temporal variability, when combined with the fact that measurements with different sensors in similar relative positions did not always replicate each other precisely, made us decide to treat the u_* data stochastically rather than deterministically. Weighted geometric averages and standard deviations of the wall and bottom shear velocities were calculated and are reported in Table 2. The weighted averages were quite robust, with standard deviations usually only a small fraction of the mean values. Further, the good fits of the 3 measured points in the D tank to linear relationships (r^2 = 0.97 for u_{*wall} vs $U_{rms,tot}$ and r^2 = 0.99 for u_{*bot} vs $U_{rms,tot}$) supported the use of linear interpolation and/or extrapolation for the remaining tanks with only 2 measured points.

Comparisons between average shear velocities and average internal mixing intensities revealed relationships that scaled with tank volume and/or shape. Average shear velocity at the bottom and wall boundaries always increased with average internal mixing intensity (F-value > 100 for both wall and bottom boundaries; Figs. 7 & 8). The mean levels of shear velocity at the bottom boundary scaled inversely with tank volume after adjustment to $U_{rms,tot}$ = 2.1 cm s^{-1} (Fig. 7). Mean adjusted u_*'s in the A and B tanks were significantly higher than in the D and E tanks. The C tank was intermediate, but it was not statistically different from any of the other tanks. New tank groups of equal volume were also compared. The new aggregated tank groups are A+B (0.1 m^3), C (1 m^3), and D+E (10 m^3). Again Tank C u_* was not statistically different from the larger or smaller tank groups, but the A+B u_* was significantly higher than the D+E u_*, with a very high confidence level (p = 0.0001). At the bottom boundary the slopes of the u_* versus $U_{rms,tot}$ regressions were statistically indistinguishable, except for the B tank, which was significantly higher (Fig. 7).

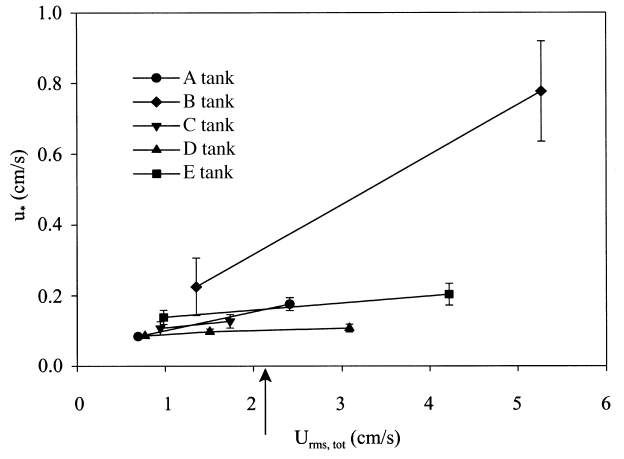

Fig. 8. Shear velocity (u_*) measured by hot-film sensors at the wall boundary versus mixing intensity ($U_{rms,tot}$) in the MEERC P/B tanks. Weighted average geometric means and standard deviations from 4 experimental runs per tank are shown; arrow shows normalizing level for comparison of mean shear velocity between tanks

At the wall boundary, a somewhat different pattern was observed (Fig. 8). The levels of shear velocity adjusted to $U_{rms,tot}$ = 2.1 cm s^{-1} were not statistically different except for B tank u_*, which was significantly higher. On the other hand, the slopes of the u_* versus $U_{rms,tot}$ regressions scaled with volume and/or shape for certain combinations of tanks. The B tank slope was significantly higher than all of the others, though it was similar to the A tank slope at p = 0.085. The aggregated slope of the smaller tanks (A+B) was significantly higher than the slope of the larger tanks (C+D+E), with a very high confidence level (p = 0.0001).

DISCUSSION

There were clear scale (volume and shape) dependencies in relationships between boundary shear velocity and internal mixing intensity in the MEERC P/B tanks. The primary reason is simply one of volume and/or size. This is apparent from Fig. 3. The longer paddles of the D tank generated more intense flow near the paddle tips than in the C tank at the same stirring rate (3 cm s^{-1} in D vs 1.3 cm s^{-1} in C). However, the larger volume but similar geometry of the D tank ensured that the paddles were much further from the boundaries. This allowed much more of the mixing energy to be dissipated in the interior of the tank before it impinged on the boundaries. The result is that the D tank had a higher average $U_{rms,tot}$ than the C tank, but lower average u_*'s at the wall and bottom boundaries (Table 2).

The overall tendencies for size and stirring rate to affect turbulent mixing in tanks are summarized well by the impeller Reynolds number, an important nondimensional parameter in chemical engineering studies of mixing processes (Tatterson 1991). The impeller Reynolds number is defined as

$$Re_D = \frac{ND^2}{\nu} \quad (7)$$

where N is the rotational speed of the paddle in revolutions s^{-1}, D is the diameter of the impeller (paddle) in cm, and ν is the kinematic viscosity in cm^2 s^{-1}. For similar mixing geometries Re_D is the dominant scaling parameter for mixing efficiency (power consumption) in stirred tank reactors (Tatterson 1991). Re_D should not be expected to completely describe scaling in our situation, because we are examining relationships within a series of dissimilar tanks (paddle width did not scale with tank volume in the otherwise similar B, C, and D tanks). Nevertheless, when the ratio $u_*/U_{rms,tot}$ at the wall and bottom boundaries was plotted against

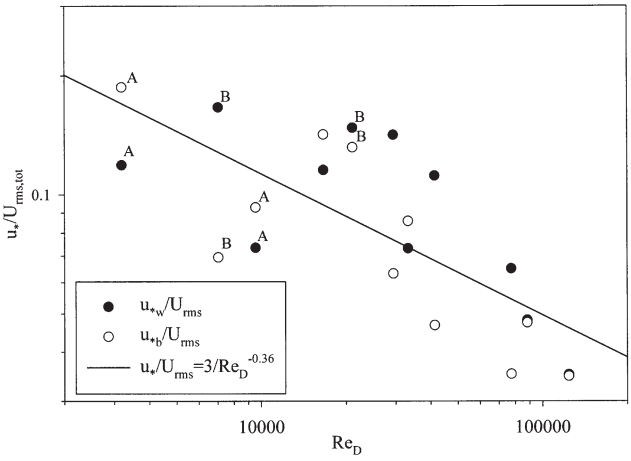

Fig. 9. Ratios of $u_*/U_{rms,tot}$ for all data from Figs. 7 & 8 plotted against impeller Reynolds number (Re_D). Line shows linear regression of the log-transformed data (r^2 = 0.55), which translates to the power law shown in the key (A and B tank points are labeled for discussion in the text)

Re_D (Fig. 9), Re_D approximately accounted for the overall volume-scaling effect.

There are 2 aspects of Fig. 9 that bear further discussion. First, the smaller (A+B) tanks all had relatively low Re_D and high $u_*/U_{rms,tot}$ values. In spite of their faster stirring rates, they had low Reynolds numbers because Re_D depends on size (D) squared. Also, as discussed above, the boundaries of the smaller tanks were closer to the paddles such that the ratio of wall shear velocity to interior mixing intensity was higher. Within this context, however, the A tanks were quite different from the others. Their ratios of $u_*/U_{rms,tot}$ were much lower than expected. If the A tank values (and one possibly errant B tank value) were removed, the slope of the best fit relationship would steepen significantly (the exponent would decrease from −0.36 to −0.61) and the scatter would be much less (r^2 would increase from 0.55 to 0.77). This implies that, while the B tank relationships appeared to be uniquely different from the others in Figs. 7 & 8, in fact the A tank relationships were the unusual ones.

We speculate that this is because the design of the A tank was significantly different from all the others. The A tank was designed to have the same volume as the B tank but also to have the same height as the C and E tanks. For adequate mixing to occur in the A tank, 5 sets of paddles needed to be used, such that the A tank had the most paddle area per unit volume of all the tanks. This may have led to a larger fraction of the total mixing energy being dissipated near the paddles in the interior, with less available for dissipation at the boundaries and therefore lower ratios of $u_*/U_{rms,tot}$. Similar considerations may explain some of the other

Table 3. Stirring rates, shear velocities and diffusive sublayer (δ_d) thicknesses for nitrogen (N) and phosphorus (P) at the wall and bottom boundaries in the MEERC P/B tanks for operational mixing rates

Tank	rpm	Wall			Bottom		
		u_* (cm s^{-1})	$\delta_{d,N}$ (mm)	$\delta_{d,P}$ (mm)	u_* (cm s^{-1})	$\delta_{d,N}$ (mm)	$\delta_{d,P}$ (mm)
A	10	0.098	1.23	0.95	0.145	0.84	0.64
B	5.75	0.161	0.75	0.58	0.024	5.03	3.87
C	3.75	0.107	1.13	0.87	0.134	0.90	0.69
D	2.25	0.088	1.37	1.06	0.038	3.17	2.44
E	2	0.139	0.87	0.67	0.062	1.94	1.50

scatter in Fig. 9, scatter that might be much less for tanks with true geometric similarity. In other words, the boundary shear velocities in the MEERC P/B tanks and similar stirred mesocosms are not necessarily a simple function of scale, but also of the design specifications of each tank.

The choice of building and using the hot-film sensors was initially made so the shear velocity within each tank could be measured at high spatial and temporal resolution, but analysis of the instantaneous readings proved to be more difficult than we had anticipated. There were some constraints on the deployment and usage of the sensors that may have contributed to these instantaneous uncertainties. The sensors were covered with approximately 1 mm of flexible plastic to protect the circuitry from the water. Any sharp boundary affecting the flow before it passed over the actual sensor might have created a developing internal boundary layer over the sensor itself, which would have compromised the data. In an attempt to minimize this experimental artifact, care was taken to create a beveled surface where the flexible plastic covering the sensor and the tank wall met, so as to minimize flow disruption. The wires which connected the sensors to the datalogger were also an experimental problem, since they may have disrupted the flow to some extent. Care was taken in placing the wires so that they disrupted flow as little as possible. The sensors and wires generally protruded <2 mm from the surrounding surface, which is significantly less than the typical thickness of the viscous sublayer at the MEERC P/B tanks solid boundaries (~1 cm at u_* = 0.12 cm s^{-1}). In any case, flow disruption and/or a developing internal boundary layer would have increased heat transfer from the sensors and resulted in an overestimate of shear velocity. In fact, we suspect that some of the variability that prevented us from using the hot-film data as originally intended was due to the extremely low shear velocities often encountered in our experiments. As stated above, a low threshold for reliable shear velocity measurements with hot-film sensors has been defined previously as 0.288 cm s^{-1} (Gust 1988). We believe that we devised a reasonable procedure to extrapolate our measurements below this value, but instantaneous readings were somewhat erratic below this threshold. Thus, although we have confidence in the space/time-averaged readings, the instantaneous readings were sometimes difficult to interpret and were not used.

The levels of shear velocity corresponding to operational mixing rates used during ecological experiments in the MEERC P/B tanks are shown in Table 3, and examples of shear velocities from the natural environment are shown in Table 4. MEERC P/B operational mixing rates were sometimes different from the experimental mixing rates used in the present work, and in these cases shear velocities were calculated using linear interpolation. The operational mixing rate for the B tank was less than the lowest experimental mixing rate, and therefore extrapolation was used to calculate shear velocity at the operational rate. The extrapolated value of u_{*b} at the B operational mixing rate is extremely low because of the large slope of the u_* versus $U_{rms,tot}$ curve for the B tank. The actual shear velocity may not have been this low, but we have no objective reason for eliminating this data point. Shear velocity levels in the MEERC P/B tanks at operational mixing rates were generally lower than in the natural environment, especially at the bottom boundary. This was expected, as the MEERC P/B tanks were designed

Table 4. Some examples of shear velocities from natural environments

Location	u_* (cm s^{-1})	Source
Atlantic Shelf	0.25–0.48	Santschi et al. (1991)
Atlantic Shelf	0.16–0.43	Santschi et al. (1991)
Smooth sea floor	0.1–1.0	Dade (1993)
Smooth sea floor	1.0	Boudreau & Guinasso (1982)
Pacific floor	0.05–0.3	Wimbush & Munk (1970)
Beneath Florida current	0.1–1.0	Weatherly (1972)
Irish Sea	0.4–2.6	Heathershaw (1976)
Temperate lake	1.0	Boudreau & Scott (1978)
Seagrass leaves	0.6–4.0	Koch (1994)

to provide realistic levels of turbulence in the water column, not at the bottom boundary.

Some examples of previously reported, natural, diffusive sublayer thicknesses are given in Table 5. In general these are on the order of 1 mm for deep-ocean sediments and smaller for coastal sediments and more energetic environments. Diffusive sublayer thicknesses for the MEERC P/B tanks were calculated using Eq. (4) for operational shear velocities and appropriate molecular diffusion coefficients. Diffusive sublayer thicknesses under normal operating conditions in the MEERC P/B tanks are given in Table 3 for nitrogen and phosphate. As nitrogen (ammonium, nitrate, and nitrite) and oxygen have similar molecular diffusion coefficients, (~1.7 and 2.0×10^{-5} cm^2 s^{-1}, respectively, at 20°C), their diffusive sublayer thicknesses are comparable. The diffusive sublayer thicknesses at the wall boundary in the MEERC tanks were similar to those found in low-energy deep-sea environments. At the bottom boundary the A and C tanks also had diffusive sublayer thicknesses similar to deep-sea environments. The B, D, and E tanks had atypically large diffusive sublayer thicknesses. None of the tanks had diffusive sublayer thicknesses similar to the more energetic coastal environments that the mesocosms were attempting to simulate.

Our experiments did not use bottom sediments. Instead, the smooth bottoms of the mesocosms were used to simulate the benthic boundary by lowering the paddles the distance usually occupied by the sediments. It is possible that operational use of sediments in MEERC P/B ecosystem experiments introduced sufficient roughness to influence shear velocity (Huettel & Gust 1992). Roughness also increases the surface area of the sediment available for interaction with the water column (Dade 1993). Therefore, sediment roughness can increase mass transfer across solid-water interfaces. The Roughness Reynolds Number can be used to determine if these effects should be important. In general if the roughness elements are larger than the viscous sublayer, then the boundary is considered rough. This was usually not the case in MEERC P/B ecosystem experiments, as the sediment was manually smoothed and macrofauna were excluded, leaving few if any roughness elements as large as the viscous sublayer (~1 cm). Thus, the large diffusive sublayer thicknesses in Table 3 were a good basis for estimating the extent of diffusion limitation of benthic-pelagic fluxes in MEERC P/B experiments.

Lower levels of turbulence at the sediment-water interface can greatly affect experimental aquatic ecosystems. The sediment-water interface is where gradients of physical, chemical, and biological properties are at their greatest (Santschi et al. 1990). Fluxes across the sediment-water boundary are determined by these concentration gradients in combination with uptake and release kinetics at the sediment surface and just below. These fluxes can influence sediment dynamics and diagenetic processes and affect biogeochemical cycles in experimental aquatic ecosystems (Boudreau & Guinasso 1982, Jørgensen & Revsbech 1985, Santschi et al. 1991, Dade 1993, Porter 1999). In fact, Sanford & Crawford (2000) have estimated that sediment-water nutrient uptake was limited by the diffusive sublayer much of the time in MEERC P/B ecosystem experiments, based on measured sediment-uptake kinetics, typical ambient nutrient concentrations, and the estimated diffusive sublayer thicknesses in Table 3.

Wall boundaries, on the other hand, are an artifact of experimental ecosystem enclosure studies. Nutrient uptake by wall periphyton reduces available nutrients in the water column for primary production by phytoplankton and for nutrient cycling to the benthos. The levels of shear velocity at the wall boundary, which are at least partly a function of the mixing design, can further complicate the situation. High levels of shear velocity at the wall boundary can magnify the problem by increasing fluxes of nutrients to the walls and inducing periphyton growth (Chen et al. 1997). Sanford & Crawford (2000) also showed that nutrient uptake at the wall boundaries in the MEERC tanks was often diffusion-limited, such that shear velocity levels controlled wall fluxes of nutrients as well as benthic fluxes.

Table 5. Some examples of diffusive sublayer thicknesses (δ_d, equivalent to film thickness, L) from natural environments

Location	δ_d or L (mm)	Scalar	Source
Deep Pacific	1.12	Gypsum	Santschi et al. (1983)
Danish Coast, 15 m depth	0.5–0.7	Oxygen	Gundersen & Jørgensen (1990)
Deep sea floor	1–2	General	Boudreau & Guinasso (1982)
Coastal environments	0.47	Gypsum	Anderson et al. (1990)
Danish Coast	0.2–1	Oxygen	Jørgensen & Revsbech (1985)
Exposed sediments	0.1–0.2	Gypsum	Santschi et al. (1983)
Model	0.7–1.9	Oxygen	Hall et al. (1989)
Seagrass leaves	0.10–0.33	Oxygen	Koch (1994)

Conclusions

Shear velocities at the interfaces of the MEERC P/B tanks were measured using hot-film sensors. Shear velocity was directly proportional to mixing in the MEERC P/B tanks. The levels of shear velocity at the bottom boundary scaled with tank volume. The smaller tanks (A+ B) had larger bottom shear velocities than the largest tanks (D+E), when adjusted to a common internal mixing intensity of 2.1 cm s^{-1}. Adjusted mean bottom shear velocities in the middle tank (C) were not statistically different from any of the others. There was no relationship between tank volume and the rate of increase in shear velocity with increased mixing at the bottom boundary. However, the slope of the B tank relationship was significantly higher than the others. At the wall boundary a somewhat different situation was observed. The levels of shear velocity adjusted to a common internal mixing intensity of 2.1 cm s^{-1} were not statistically different except for the B tank, which had significantly higher wall shear velocity. On the other hand, the rate of increase in wall shear velocity with increased mixing scaled with volume and/or shape for certain combinations of tanks. The B tank slope was significantly higher than all of the others, and the aggregated slope of the smaller tanks (A+B) was significantly higher than the slope of the larger tanks (C+D+E).

A bulk impeller Reynolds number captured some of the volume/size-dependence of ratios of boundary shear velocity to internal mixing intensity. Physically, the observed decreasing trend in ratios of boundary shear velocity to internal mixing intensity with increasing Reynolds number was most likely due to increasing internal dissipation of mixing energy in the larger tanks combined with increasing distances between the paddles and the boundaries. However, differences in tank geometry and mixing design resulted in significant shortcomings in the Reynolds number scaling; mixing design and tank geometry were also important. In particular, the tall, thin A tank appeared to have a lower ratio of boundary shear velocity to internal mixing intensity than expected on the basis of the Reynolds number scaling.

Levels of boundary shear velocity in the MEERC P/B tanks were considerably lower than levels in the natural environment. The fluctuating flow at the bottom of the MEERC P/B tanks did not produce the same levels of shear velocity as in the natural environment at realistic levels of internal mixing. The wall boundary layers had diffusive sublayer thicknesses, similar to observations from deep-sea environments, while the benthic diffusive sublayer thicknesses were even larger. The benthic boundary layers in the MEERC tanks did not mimic boundary layers typical of energetic coastal environments. Most current mesocosm designs that include mixing are likely to be affected similarly. At the time this was written, there were no operational mesocosm designs that accurately simulate natural benthic-boundary layers and water-column turbulence at the same time (but see Porter 1999). An artificially low-energy benthic environment may have important consequences for ecosystem processes affected by pelagic-benthic coupling. For the results from experimental ecosystem-enclosure studies to be more accurate, these artifacts of mixing in enclosures need to be better understood, quantified, and subsequently minimized.

Acknowledgements. We thank the many friends and colleagues whose valuable help was integral to data collection and analysis, especially S. Suttles and E. Porter, and we thank J. Cornwell, E. Koch, and 3 anonymous reviewers for their careful reviews and helpful suggestions. This research was supported by the Multiscale Environmental Ecosystem Research Center (MEERC) at the University of Maryland Center for Environmental Science (UMCES) through the US Environmental Protection Agency STAR program, grant no. R 819640. UMCES publication number 3395.

LITERATURE CITED

Anderson R, Fleisher M, Santschi PH (1990) Measurements of diffusive sublayer thicknesses in the ocean by alabaster dissolution and their implications for the measurements of benthic fluxes. EOS Trans Am Geophys Union 71/2:124

Batchelor GK (1967) The theory of homogenous turbulence, 5th edn. Cambridge University Press, Cambridge

Boudreau BP, Guinasso NL (1982) The influence of a diffusive sublayer on accretion, dissolution, and diagenesis at the seafloor. In: Fanning KA, Manheim FT (eds) The dynamic environment of the ocean floor. DC Heath and Company, Lexington, p 115–145

Boudreau BP, Scott MR (1978) A model for the diffusion-controlled growth of deep-sea manganese nodules. Am J Sci 278:903–929

Chen CC, Petersen JP, Kemp WM (1997) Spatial and temporal scaling of periphyton growth on walls of estuarine mesocosms. Mar Ecol Prog Ser 155:1–15

Dade WP (1993) Near-bed turbulence and hydrodynamic control of diffusional mass transfer at the sea floor. Limnol Oceanogr 38:52–69

Gundersen JK, Jørgensen BB (1990) Microstructure of diffusive boundary layers and the oxygen uptake of the seafloor. Nature 345:604–607

Gust G (1988) Skin friction probes for field applications. J Geophys Res 93:14121–14132

Gust G, Muller V (1997) Interfacial hydrodynamics and entrainment functions of currently used erosion devices. In: Burt N, Parker R, Watts J (eds) Cohesive sediments. Wiley & Sons Ltd, Chichester, p 149–173

Hall POJ, Anderson LG, Rutgers van der Loeff MM, Sundby B, Westerlund SFG (1989) Oxygen uptake kinetics in the benthic boundary layer. Limnol Oceanogr 34:734–746

Heathershaw AD (1976) Measurements of turbulence in the Irish Sea benthic boundary layer. In: McCave IN (ed) The benthic boundary layer. Plenum, New York, p 11–31

Huettel M, Gust G (1992) Impact of bioroughness on inter-

facial solute exchange in permeable sediments. Mar Ecol Prog Ser 89:253–267

Jørgensen BB, Des Marais DJ (1990) The diffusive boundary layer of sediments: oxygen microgradients over a microbial mat. Limnol Oceanogr 35:1343–1355

Jørgensen BB, Revsbech NP (1985) Diffusive boundary layers and the oxygen uptake of sediments and detritus. Limnol Oceanogr 30:111–122

Koch EW (1994) Hydrodynamics, diffusion-boundary layers and photosynthesis of the seagrasses *Thalassia testudinum* and *Cymodocea nodosa*. Mar Biol 118:767–776

Kraus NC, Lohrmann A, Cabrera R (1994) New acoustic meter for measuring 3D laboratory flows. J Hydraul Engin 20: 406–412

Langley R (1968) Practical statistics. Dover Publications Inc, New York

Nowell ARM, Jumars PA (1984) Flow environments of aquatic benthos. Annu Rev Ecol Syst 15:303–328

Petersen JE, Sanford LP, Kemp WM (1998) Coastal plankton responses to turbulent mixing in experimental ecosystems. Mar Ecol Prog Ser 171:23–41

Porter ET (1999) Physical and biological scaling of benthic-pelagic coupling in experimental ecosystem studies. PhD dissertation, University of Maryland, College Park

Porter ET, Sanford LP, Suttles SE (2000) Gypsum dissolution is not a universal integrator of 'water motion'. Limnol Oceanogr 45(1):145–148

Rahm L, Svensson U (1989) On the mass transfer properties of the benthic boundary layer with an application to oxygen fluxes. Neth J Sea Res 24:27–35

Riber HH, Wetzel RG (1987) Boundary layer and internal diffusion effects on phosphorus fluxes in lake periphyton. Limnol Oceanogr 32:1181–1194

Sanford LP (1997) Turbulent mixing in experimental ecosystem studies. Mar Ecol Prog Ser 161:265–293

Sanford LP, Crawford SM (2000) Mass transfer versus kinetic control of uptake across solid-water boundaries. Limnol Oceanogr 45(5):1180–1186

Santschi PH, Bower P, Nyffler UP, Azvedo A, Broecker WS (1983) Estimates of the resistance to chemical transport posed by the deep-sea boundary layer. Limnol Oceanogr 28:899–912

Santschi PH, Hohener P, Benoit G, Buchholtz-ten Brink M (1990) Chemical processes at the sediment-water interface. Mar Chem 30:269–315

Santschi PH, Anderson RF, Fleisher MQ, Bowles W (1991) Measurements of diffusive sublayer thicknesses in the ocean by alabaster dissolution, and their implications for the measurements of benthic fluxes. J Geophys Res 96:10 641–10 657

Snelgrove PVR, Butman CA (1994) Animal-sediment relationships revisited: cause versus effect. Oceanogr Mar Biol Annu Rev 32:111–117

Tatterson GB (1991) Fluid mixing and gas dispersion in agitated tanks. McGraw-Hill Inc, New York

Tennekes H, Lumley JL (1972) A first course in turbulence. MIT Press, Cambridge

Weatherly GL (1972) A study of the bottom boundary layer of the Florida Current. J Phys Oceanogr 2:54–72

Wimbush AHMH, Munk W (1970) The benthic boundary layer. In: Maxwell AE (ed) The sea, Vol 4. Wiley & Sons, Inc, New York, p 3–10

Editorial responsibility: Otto Kinne (Editor), Oldendorf/Luhe, Germany

Submitted: October 13, 1998; Accepted: June 20, 2000
Proofs received from author(s): January 9, 2001